Applied Catalysis B: Environmental 238 (2018) 568–575

Contents lists available at ScienceDirect

Applied Catalysis B: Environmental

journal homepage: www.elsevier.com/locate/apcatb

Under vacuum synthesis of type-I heterojunction between red phosphorus and graphene like carbon nitride with enhanced catalytic, electrochemical and charge separation ability for photodegradation of an acute toxicity category-III compound

Tahir Muhmood, Mingzhu Xia*, Wu Lei, Fengyun Wang*

School of Chemical Engineering, Nanjing University of Science and Technology, Nanjing, 210094, Jiangsu, PR China

ARTICLE INFO

Keywords:
Vacuum tubes
Metsulfuron methyl
Red phosphorus
Graphitic carbon nitride
Electrochemical

ABSTRACT

In this study, we reported a novel type-I heterojunction between red phosphorus and graphitic carbon nitride under vacuum condition, which is a novel synthesis process. For preparing the red phosphorus composites, the vacuum condition is appropriate to prevent it from self-ignition. The prepared materials were analyzed with different analytic techniques for the confirmation of their heterojunctions and structure formation. The introduction of red phosphorus into graphitic carbon nitride, reduce the structural defects and increase the charge separation ability. After medication, the synthesized composite shows an enhanced photocatalytic activity against acute toxicity category-III non-color (MTSM, Metsulfuron methyl) and color (RhB), organic pollutants. The photocatalytic degradation mechanism (Mott-Schottky and VB-XPS) study reveal that red phosphorus /graphitic carbon nitride possess type-I heterojunction with enhanced catalytic behavior, due to the effective transformation of photo-generated electrons from CB of GCN to CB of RP with the help of heterojunctions and due to unmoved photo holes on VBs. Synthesized composites also maintained their performance after reused them in three cyclic form.

1. Introduction

Photocatalysts have attracted much more research attention in these years due to their design and their workability, maximum in the solar range [1,2]. The large amount of waste and disproportionate use of sulfonylurea pesticides such as metsulfuron methyl (MTSM) in agriculture cause the main contaminations. MTSM is used for killing the weeds and grasses from the fields. It possesses the toxic for living organisms (mammals, fish, birds and insects) and also cause eye irritation [3]. Environmental hazards and energy problems can be solved with the help of photocatalysts [4]. Voluntarily photocatalysts efficiently work as, degradation of the organic pollutants [5], water splitting [6,7] and solar cell [8]. Some visible light photocatalysts such as, $BiVO_4$ [9], $CuIn_xGa_{1-x}Se_2$ [10], and $BiOI/CaBi_2O_2(CO_3)_2$ [11] have been synthesized and enact excellent performance. Analyze these complicated photocatalysts with some elemental semiconductors which have simpler compositions, including sulfur [12] and red phosphorus [13] have attracted much attention in recent years. These elemental semiconductors (sulfur, red phosphorus) have distinctive advantages included, absorption of a wider range of visible light, economical and earth-abundant [14]. Among them the red phosphorus is considered as a strong photocatalysis agent in visible light because it is a stable semiconductor with band gap energy 1.7 eV, absorb visible light [15], possess good stability and low cost, thus it can make more efficient heterojunction with other materials [16]. It also has different chemical forms and structure such as tubular, fibrous, and amorphous. Researchers also found that all these forms of red phosphorus possess the photo-catalytic behavior [17]. Some research groups also reported that the fiber-like red phosphorus has highest PHE (photocatalytic hydrogen evolution) in the elemental family of photocatalysts [18]. In another view, some restriction also exists in its photocatalytic activity due to high e^-/h^+ charge recombination rate over red phosphorus (RP) and its low surface area [19]. For resolving this problem different material such as black phosphorus, metals and carbon-based materials previously have been coupled with RP leading to a steep increase in photocatalytic ability [20]. Recently the phosphorus was used for making a composite with TiO_2 for improvement in catalytic performance [21]. On the other hand graphitic carbon nitride ($g\text{-}C_3N_4$) has attracted

* Corresponding authors.
E-mail addresses: 863271491@qq.com (M. Xia), ind-chem-njust@foxmail.com (F. Wang).

https://doi.org/10.1016/j.apcatb.2018.07.029
Received 7 May 2018; Received in revised form 22 June 2018; Accepted 9 July 2018
Available online 18 July 2018
0926-3373/

worldwide attention as a metal-free photocatalyst and it can absorb visible light [22,23]. The physiochemical stability of g-C_3N_4 and its synthesis process, makes it suited for degradation of organic pollutants [24,25]. Still researchers are doing improvements in g-C_3N_4 efficiency by using various changes such as doping with metal, non-metal and composite with other semiconductors, and also included, changing in its morphology [26,27]. The g-C_3N_4 based composites are considered as a perfect material for the energy and catalytic properties. It is commonly synthesized from nitrogen-rich precursors such as, urea, trithiocyanuric acid, cyanamide, melamine, dicyandiamide and thiourea by simple pyrolysis method [28]. Researchers have made some modification and established various strategies to control it fast charge recombination rate by synthesizing composite, doping with metals and deposition of metals. Heterojunction between appropriate semiconductors is an effective technique to enhance the photocatalytic ability. In our above assessment, it's required to synthesize a novel heterojunction between red phosphorus and graphitic carbon nitride with a novel method which owns the properties such as; narrow band gap, intensive visible light absorption ability with charge storage ability and a large number of charge carrier that may participate in the photocatalytic reaction. Consequently, in our current work, taking the enhancement advantages of RhP and g-C_3N_4, we prepared the type-I heterojunctions between them under vacuum condition by using sealing the materials into the vacuum tubes (a facile and novel method), for an effective and visible light driven photocatalyst which have the ability to degrade the non-color (MTSM, Metsulfuron methyl) and color (RhB, Rhodamine-b) organic pollutants.

2. Experiment detail

All chemical were purchased from the SigmaAldrich and used without further purification. The graphitic carbon nitride (GCN) was synthesized with polymerization method using melamine as a precursor. Typically 4 g of precursor added in a covered quartz crucible and put it in a muffle furnace for 4 h at 520 °C. After that crush the product for further use. For preparation of heterojunctions between red phosphorus (RP) and graphitic carbon nitride (GCN), their different weight percentage ratios (RPCN-1 = 15%RP, RPCN-2 = 30%RP, RPCN-3 = 45%RP) were milled in agitator mortar for a half hour and then sealed in an evacuated Pyrex quartz tube under vacuum condition (as shown in Fig.1 and Fig.S1) The vacuum tubes are heated at 600 °C for 7 h in furnace. After cooling down naturally at room temperature, open the tube in an argon-filled glove box. After that used the material for characterizations and further.

2.1. Characterization

Bruker D8-X-Ray-Diffractometer with Cu-Kα radiation in the range of 5-60° (2Θ) was used for X-ray-diffraction measurements. Scanning-Electron-Microscopy (JEOL JSM-6380LV) and Transmission-Electron-Microscopy (JEM-2010) at different magnifications were used for analyzing the morphology of prepared materials. The photocatalysis process for the measurements and checking the degradation ability of materials was done in the photochemical reactor (BL-GHX-1D Shanghai-Bilon-Instrument Co. Ltd.) with xenon arc lamp (XBO, 500 W). Degradation quantitative measurements of MTSM and RhB were done with the help of UV–vis spectrophotometer (Thermo-Fisher-EV220, USA). Fourier-transform-infrared spectra (FT-IR) were noted by Thermo-FisherNicolet-iS10-FT-IR spectrometer. The electrochemical analyzer (ChenHua-Instruments-Shanghai, P.R.China) with standard three electrodes was used for photo-electrochemical measurements. X-ray photoelectron spectroscopy (XPS) measurements were performed on ESCALAB-250Xi (Thermo Fisher Scientific USA) using a PHI Quantera-II spectrometer, with Al Kα (1486.6 eV) radiation. Electron spin resonance (ESR) of the spin-trapped paramagnetic species with DMPO were tested by the Bruker Elexsys E500 spectrometer (Billerica, MA, USA)

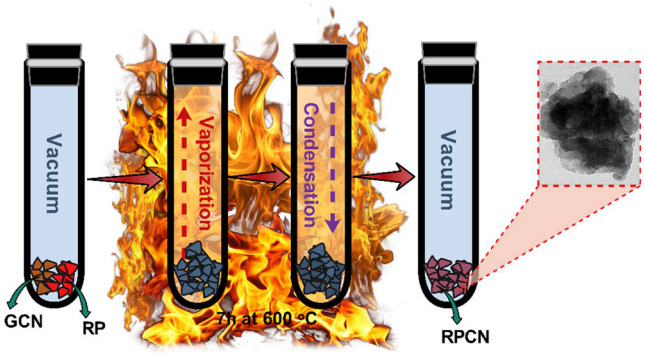

Fig. 1. Schematic representation of RPCN synthesis.

2.2. Photo-electrochemical (PEC) measurement

The PEC measurements were performed by the electrochemical analyzer. In these measurements, the Na_2SO_4 solution (0.5 M) worked as the electrolyte. The platinum wire used as counter electrode and Ag/AgCl electrode work as a reference electrode. The ITO (Indium tin oxide) glass slides (5 mm^2) were used as working electrode. For analysis, add 3 mg of sample into 1 ml ethanol and sonicate it for 15 min. Then 0.10 ml of sample suspension was dropped onto the conductive side of ITO glass and dry it for 10 h at 40 °C. For the light source, a 300 W Xe-Lamp was used. The working electrode and lamp have 30 cm distance.

2.3. Adsorption and photo-catalytic experiment

The prepared materials photocatalytic activity was investigated by the degradation of MTSM and RhB in a photochemical reactor. 15 mg of as prepared catalyst was added into 45 ml of prepared pollutant solutions (MTSM and RhB separately) (MTSM = 15 mg/L, RhB = 15 mg/L) in a glass tube. Stirrer this suspension in dark for 45 min for the measure of adsorption capacity. After 35 min, turn ON the photo-chemical reactors Xenon-arc-lamp (500 W, 420–720 nm, cutoff filter). The distance between lamp and target sample glass tube is almost 5 cm. This whole photocatalysis process in the photochemical reactor was done under continuous stirring. For analysis, the degradation rate 4–5 ml of solution was extracted carefully. The removed solution was centrifuged at 12,000 rpm for 20 min to check the stability of catalysts by reusing them.

3. Results and discussion

The XRD (X-ray diffraction) pattern in fig.2 represents the phase composition and structure of prepared composites of red phosphorus (RP), g-C_3N_4 (GCN), RPCN-1, RPCN-2, and RPCN-3. One distinct peak at 15.3° corresponding to 102 planes was founded which is akin to the literature and representing a medium range ordered structure of commercially available RP [29]. Other two characteristic peaks, one at 13.1° consigned to the inter-planar staking of aromatic units and second at 27.5° consigned to the crystal plane of graphitic like material, are signature for the GCN [30]. There is no other new phase in XRD-pattern of heterojunction composites. Presence of all these three peaks in XRD-pattern of prepared composites confirmed the successful erection of the structure. From the literature, it can easily explain that commercially available red phosphorus is broken down into a small size and the g-C_3N_4 sheet can also form due to the mechanical grinding [31]. The FT-IR analysis (fig.3) also confirmed that the original GCN backbones remain unaffected after heterojunction composite formation with RP and no vibrational peak of RP [32,33] related group in composites (RRPCN-

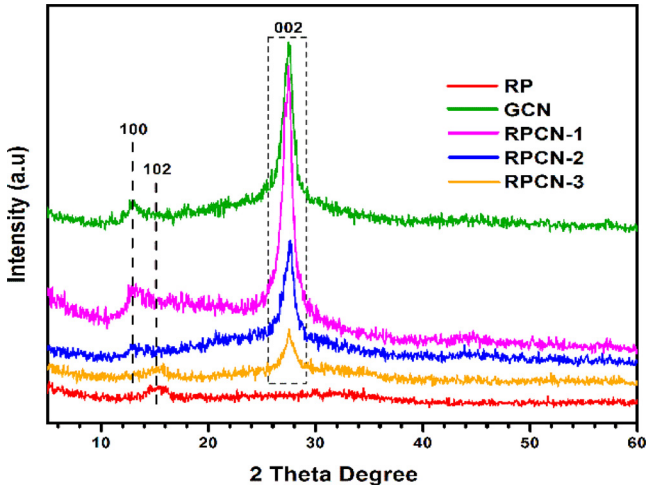

Fig. 2. XRD pattern of RP, GCN, RPCN-1, RPCN-2, and RPCN-3.

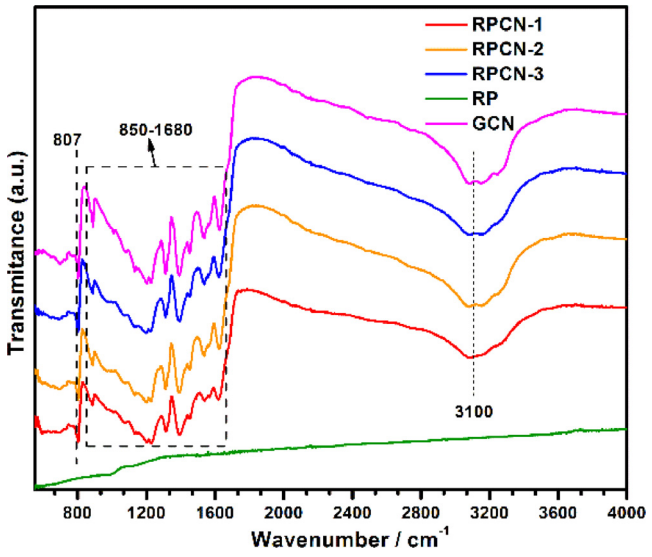

Fig. 3. FTIR of RP, GCN, RPCN-1, RPCN-2, and RPCN-3.

1, RPCN-2, RPCN-3) representing that the vacuum tube method unlikely initiates new chemical bonding between RP and GCN. The main fingerprints of GCN are observed between 850 cm^{-1} to 1680 cm^{-1} and were allocated to stretching-vibration of hepatize rings, mostly the C═N (sp^2) stretching and C−N (sp^3) out-of-plane vibration.

The sharp peak at 807 cm^{-1} was assigned to the breathing mode of tris-s-triazine rings. While the broader peak at 3100 cm^{-1} is assigned to the stretching vibration due to the residual N−H units and O−H unites (due to adsorbed water species) [34]. The physiochemical properties of prepared catalysts were analyzed with the help of UV–vis diffuse absorbance spectroscopy, shown in fig.4a. The vital characteristic absorption edge of GCN appear at 450 nm and for RP appear at 700 nm [35]. The UV–vis spectrum of RPCN-1, RPCN-2 and RPCN-3 display blended absorption features of RP and GCN [30]. The absorption edge of GCN becomes more prominent in composites with the increase of GCN amount in RPCN. The band gap was calculated with the help of Kubelka-Munk *vs* Eg (band gap energy) as shown in Fig.4a such as 1.61 eV for RP, 2.72 eV for GCN and 2.36 eV for RPCN-3. An additional lower Eg 1.65 eV was also observed in RPCN-3 which may be due to the conduction band tail states owning the impurities that lower the CB minimum range as reported in the literature for narrowing the TiO_2 band gap [36]. The composites RPCN-1, RPCN-2, and RPCN-3 showed expressively enhanced absorption in visible region which may be due to the mutual synergistic effects of narrow band-gap and light absorbance characteristic of RP and GCN. These results specify that RPCN-heterostructures are highly advantageous for photocatalysis because they are active in a broad range of visible light region and can produce charge carrier under visible light irradiation.

The PL spectrum of GCN (Fig.4b) shows an intense emission peak between 400 nm–650 nm and maximum peak at 460 nm in the blue area. The interfacial charge transfer might be fascinated by decreased photoluminescence (PL) intensity in RPCN-heterostructures as compare to the pure graphitic carbon nitride (GCN). The PL spectrum intensity is directly related to the recombination rate of photogenerated electrons and holes. The lower PL peak intensity means the improvement in charge trapping and transferring, therefore charge carrier lifetime becomes extended and enhance the photocatalytic activity.

The X-ray photoelectron spectroscopy (XPS) analysis was used for the investigation of composition and chemical bonding between the materials during composite formation. The full scan spectrum confirms that no other element is present so no new species is generated during the experimental process. Fig.5b show the P 2p deconvoluted peaks of RP and RPCN-3 at 129.5 eV (P $2p_{3/2}$) and 130.2 eV (P $2p_{1/2}$). The comparison of N1 s deconvoluted spectrums in fig.5a indicated the shifting of binding energy from 398.1 eV, 399.8 eV and 403.7 eV (GCN) to 398.3 eV, 399.9 eV and 403.9 eV (RPCN-3) respectively. Similar the comparison of C1 s spectrum in Fig.S2 show the shifting of binding energy from 284.5 eV and 287.8 eV (GCN) to 284.8 eV and 288.0 eV (RPCN-3) respectively. The higher shift in binding energies was due to the electronic interactions that occur during the experimental process which proof the heterojunction formation between RP and GCN [37]. The morphology of as-prepared catalysts was inspected with TEM and

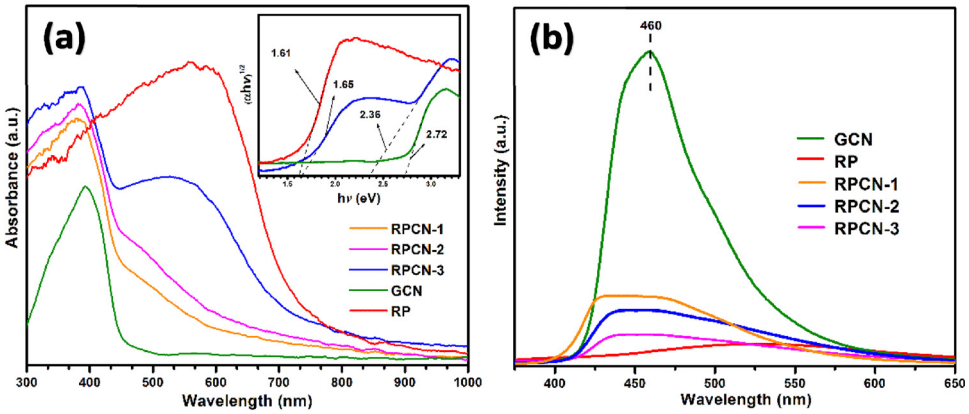

Fig. 4. (a) UV–vis absorption spectrum of RP, GCN, RPCN-1, RPCN-2 and RPCN-3, Band gap of GCN, RP and RPCN-3 (b) PL spectrum of RP, GCN, RPCN-1, RPCN-2, and RPCN-3.

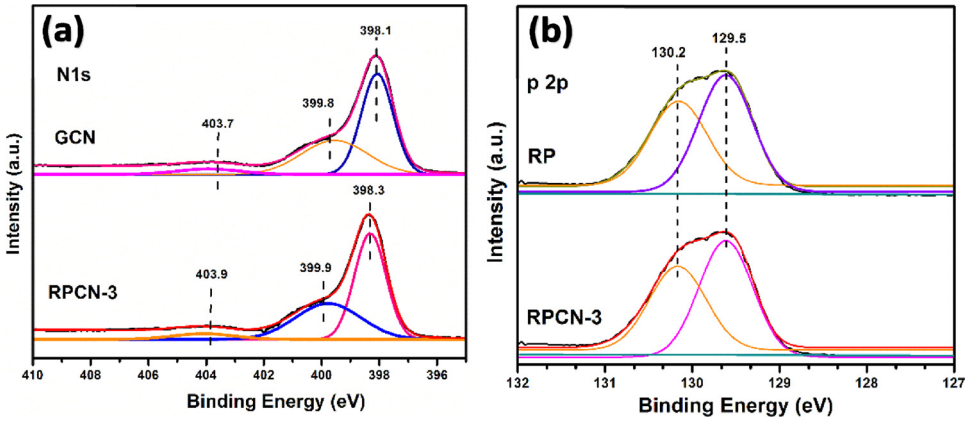

Fig. 5. XPS spectrum (a) N 1 s of GCN and RPCN-3 (b) p 2p of RP and RPCN-3.

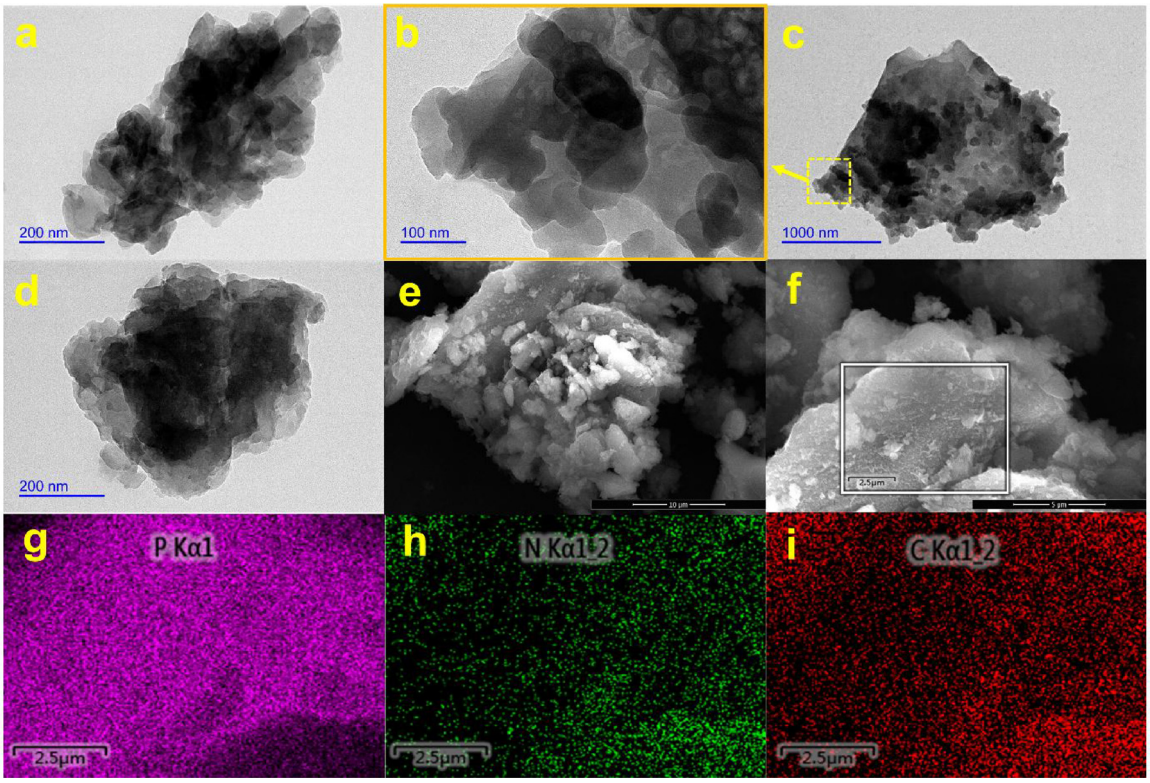

Fig. 6. TEM images: (a) RPCN-1, (b) magnified TEM image of RPCN-3, (c) RPCN-3, (d) RPCN-2, (e)(f) SEM images of RPCN-3, SEM/EDX elemental mapping of (g) P (h) N (i) C.

SEM (Fig.6). The TEM images (fig.6a-6d) of RPCNs at different magnifications evidently shows the RP existence on GN layers in an irregular form. Scanning electron microscopy (SEM) images also expose the presence of RP on GCN surface (Fig. 6e,f). SEM- elemental mapping (Fig. 6g–i) results confirm the presence of carbon, nitrogen, and phosphorus in composites. The energy-dispersive X-ray spectroscopy (EDS) spectrum (fig.S3) of RPCN-3 further approved the presence of RP.

These results fully verified the heterojunctions formation between GCN and RP. According to Mott-Schottky (Fig. 7) the flat band potential for RP was -0.33 V and for GCN was -1.45 V. With the help of Nernst-equation these potentials can be converted into RHE (reversible hydrogen electrode) and then calculated the conduction band (CB), -0.25 eV for RP and -0.85 eV for GCN. The VB edge was also examined with the help of VB-XPS. As shown in Fig.S4 with VB-XPS, the VB maxima of GCN and RP are revealed to be 1.85 eV and 1.35 eV respectively. For the probable photocatalytic mechanism, the degradation process of MTSM and RhB was done in the presence of scavengers such as Isopropanol (IPA), 1-4-benzoquinone (BQ) and ethylenediaminetraacetic acid disodium (EDTA-2Na) was used for trapping the active species hydroxyl radical (·OH), superoxide radical ($\cdot O_2^-$) and holes (h^+) respectively. The MTSM and RhB photodegradation rate under visible become majorly suppressed due to the addition of EDTA-2Na and Isopropanol. In fig.S5 trapping experiment results indicated that the OH and h^+ play a major role in degradation and $\cdot O_2^-$ play a second major role in the degradation of target organic pollutants. For further verification of photocatalytic reaction species ($\cdot O_2^-$, ·OH) the electron spin resonance (ESR) test was performed, in which DMPO (5,5-dimethyl-1-pyridine N-oxide) used as radical scavenger. In fig.S6, no characteristic peaks of DMPO($\cdot O_2^-$) and DMPO(·OH) were observed in blank test (without light irradiation). The DMPO($\cdot O_2^-$) and DMPO(·OH) characteristic peaks are present in GCN and RPCN-3 in fig.S6. Furthermore, the peaks intensity comparison between GCN and RPCN-3

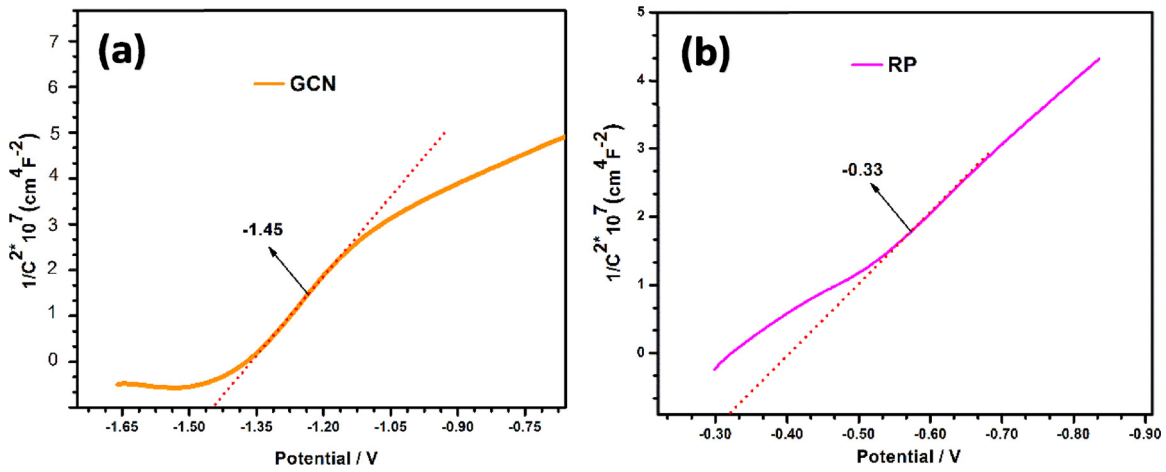

Fig. 7. The Mott-Schottky plot collected for (a) GCN (b) RP at a frequency of 1000 Hz in the dark.

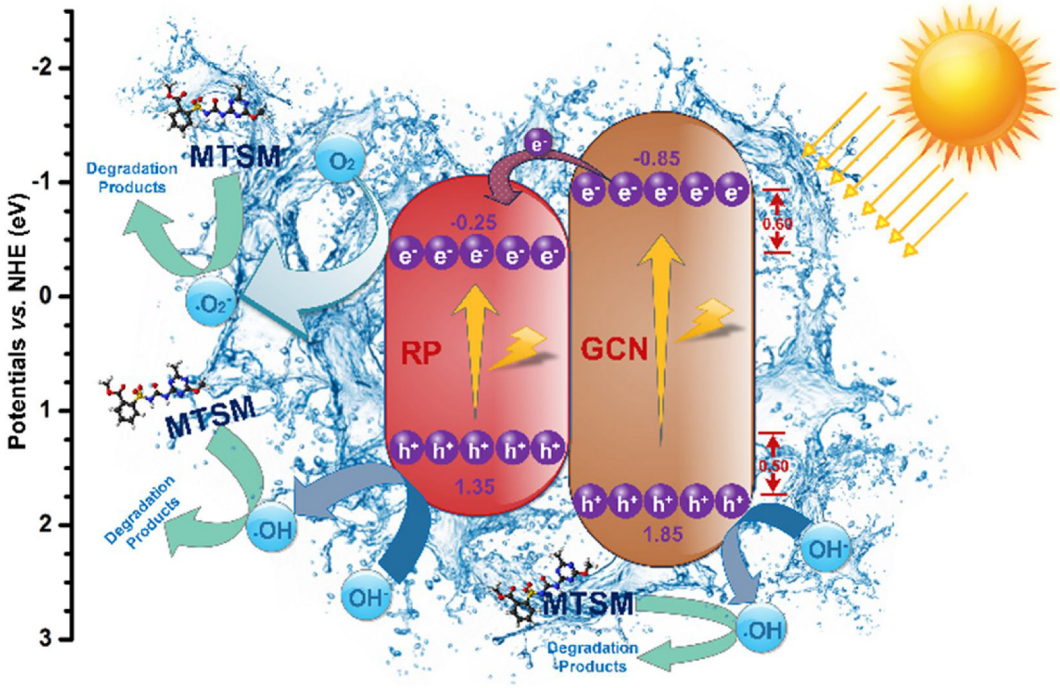

Fig. 8. Schematic of photo-generated charge transfer in RPCN-3 under visible light irradiation.

reveal that RPCN-3 exhibit strongest intensities in contrast to solo GCN which indicates that more hydroxyl and superoxide radical are produces in composite. Therefore, it can conclude that $\cdot O_2^-$, ·OH are produced during photocatalytic reaction and play important role toward degradation of MTSM and RhB under visible light irradiation accordance to ion-trapping experiment. The band diagram shows (fig.8) that heterojunction was created between red phosphorus and graphitic carbon nitride in RPCN is a type-I heterojunction. The improved catalytic behavior of RPCN-3 is due to charge transfer between RP and GCN through heterojunctions. The conduction band (CB) edge potential of GCN is more negative than RP, which help the movement of a photogenerated electron from the conduction band of GCN to the conduction band of RP under visible light irradiation. On the other hand, the photogenerated holes cannot move from valence band (VB) of RP toward VB of GCN because of more negativity of VB of RP than VB of GCN. Due to the transformation of these photogenerated electrons via heterojunctions and generation of holes on each VB, it reduces the charge recombination rate and provides a larger quantity of electrons and holes on the surface of photocatalysts.

The oxygen molecules dissolve in water captured the photogenerated electrons on photocatalyst surface and formed the radical anion ($\cdot O_2^-$) while the holes react with OH ions to form active HO·. These radical species are responsible for the photo-degradation of pollutants [38].

3.1. Photocurrent

For the quantitative study about the efficiency of photo-generated carriers in materials, the photoelectrochemical analysis is most sensitive and best technique. In Fig.9 the ON/OFF response to visible light by the prepared materials can be seen and the measurements show that the composites (RPCN-1, RPCN-2, RPCN-3) meaningfully have enhanced photocurrent as compare to the solo RP and GCN. The photocurrent response for RPCN-3 (0.26 μA/cm^2) is 2-times as high as that of RP electrode (0.14 μA/cm^2) due to type-I heterojunction between RP and GCN. The photocurrent values for RPCN-1 and RPCN-2 are 0.22 μA/cm^2 and 0.24 μA/cm^2 respectively. The photocurrent results indicated that the recombination rate of photo-generated electrons and

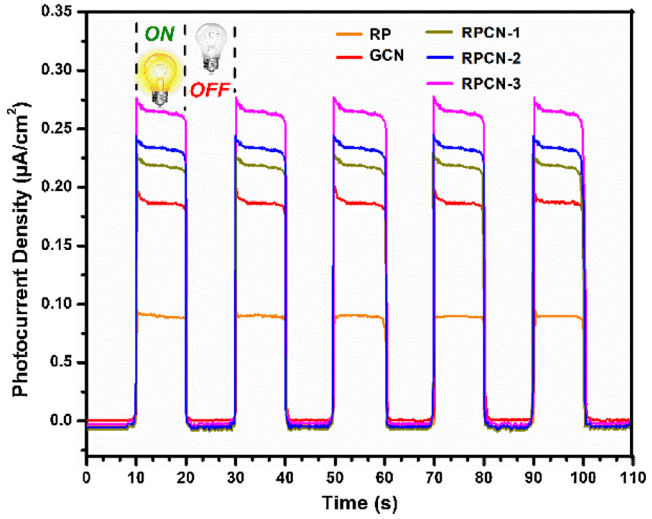

Fig. 9. Photo-current behavior of RP, GCN, RPCN-1, RPCN-2, and RPCN-3.

holes become inhibited due to the formation of a heterojunction between RP and GCN. These results also persistent the photo-catalytic results.

3.2. Photo-catalytic tests

The photo-catalytic activity as-prepared catalysts were evaluated for the degradation of metsulfuron methyl (MTSM) and rhodamine b (RhB). The photo-degradation of colored pollutants may also due to the sensitization effect, therefore to confirm the photocatalysis process without involvement of sensitization phenomena, non-colored (metsulfuron methyl) was used. The MTSM degradation by RPCN-3 curves are shown in fig.10a and fig.11a and RhB degradation by RPCN-3 curves is shown in fig.10b and fig.11b. After 35 min stirring in dark the amount of absorbed RhB and absorbed MTSM are different on different heterojunction composites. The traditionally prepared GCN showed the lowest adsorption ability. The MTSM and RhB were degraded under visible light irradiation to some extent as can be seen in blank test (without using any photo-catalyst). The GCN shows low photo-catalytic performance as compare to composites RPCN-1, RPCN-2 and RPCN-3 under visible light irradiation in a photochemical reactor. In an individual analysis of heterojunction composites, the RPCN-3 shows high photo-degradation performance for both target pollutant compounds RhB and MTSM. Under visible light irradiation, the RPCN-3 attain the complete degradation of RhB and MTSM after 120 min and 90 min respectively.

For better understanding, the photo-catalytic activity, the rate constant (k) was also found by the previously reported method. A linear relationship graph, $\ln(C/C_o)$ vs time (t) are shown in Fig.10. The rate constant for the photodegradation of MTSM over GCN, RPCN-1, RPCN-2 and RPCN-3 heterojunction composites were 0.00340 min^{-1}, 0.00804 min^{-1}, 0.01328 min^{-1} and 0.03935 min^{-1} respectively (fig.10a). While The rate constant for the photodegradation of RhB over GCN, RPCN-1, RPCN-2 and RPCN-3 heterojunction composites were 0.00282 min^{-1}, 0.00660 min^{-1}, 0.01109 min^{-1} and 0.02960 min^{-1}

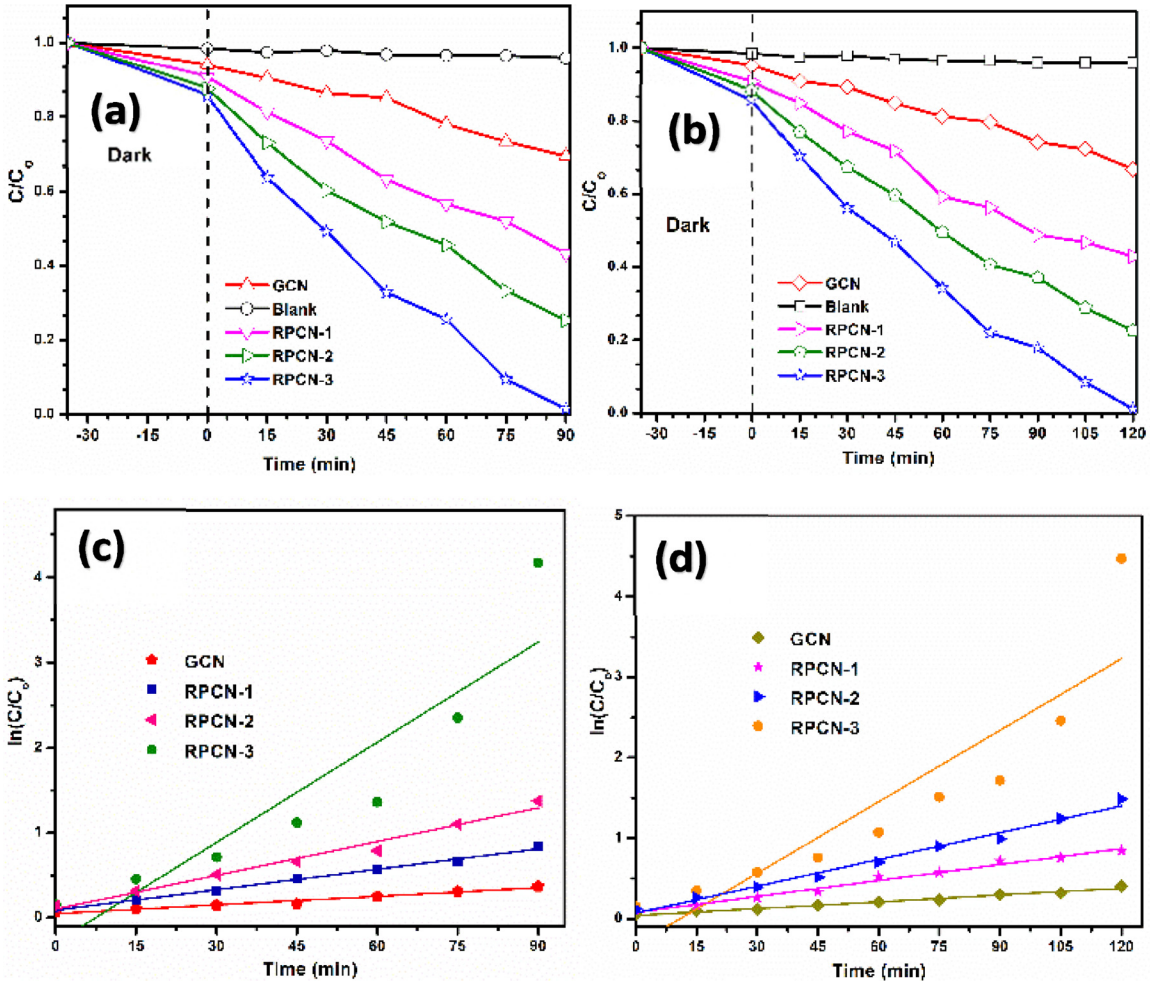

Fig. 10. Photo-catalytic degradation of (a) MTSM (b) RhB. Plots of $\ln(C/C_0)$ vs. time for (c) MTSM (d) RhB degradation.

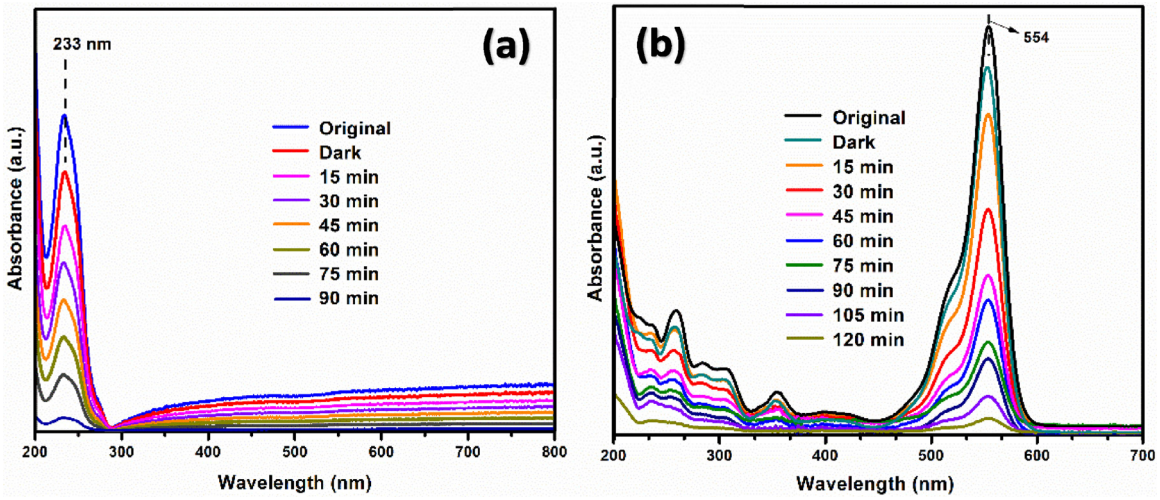

Fig. 11. Full scan degradation spectrum of (a) MTSM (b) RhB.

respectively (fig.10b). The rate constant for RhB and MTSM degradation by RPCN-3 is much higher as compare to other heterojunction composites. The successful degradation of metsulfuron methyl proof the core photocatalytic activity because MTSM is colorless and it cannot be sensitized by visible light irradiation. The GCN possess the low degradation ability in visible light irradiation because only a small number of photo-generated charge carrier joined the photocatalysis and remaining charge carrier favor the recombination. These results indicated the RPCN-3 improved photocatalytic ability for the degradation of colored (RhB) and non-colored (MTSM) organic compounds under akin photocatalysis conditions. The recycling analysis was also conducted by reusing the catalysts (collect, wash and dry) in a continuous cyclic form and the results showed (fig.S7) that the prepared catalysts possess good stability which indicates its good reusability. The RPCN-3 shows the higher photocatalytic behavior because it have type-I heterojunction and due to this the oxidative holes in RPCN-3 remain in well-kept form, so type-I RPCN-3 heterojunction possesses the higher oxidative ability and photocatalytic act.

4. Conclusion

A novel vacuum condition method was used for the preparing of the type-I heterojunction between red phosphorus and graphitic carbon nitride for the photodegradation of color (RhB) and non-color (MTSM, an acute toxicity category-III compound) organic compounds. The analytical results indicated that a successful type-I heterojunction was created which help to move the electrons from g-C_3N_4 toward Red-phosphorus and keep the holes unmoved (hole not migrate between VBs) due to their edge potential difference. The photodegradation result indicated that synthesized composited of RP and GCN (RPCN-3) degrade the MTSM (in 90 min) and RhB (in 120 min) as compared to solo graphitic carbon nitride, RPCN-2 and RPCN-1. This photo-generated charge separation ability enhanced the catalytic activity of composite and degraded the target material in short duration of time under the visible light. Recycling test indicated that prepared composites keep its stability for three reused cyclic form.

Acknowledgments

This work was financially supported by the National Natural Science Foundation of China [51472121, 51572127, 51572130 and 51672134], PAPD of Jiangsu Province, and the program for Science and Technology Innovative Research Team in Universities of Jiangsu Province, China.

Appendix A. Supplementary data

Supplementary material related to this article can be found, in the online version, at doi:https://doi.org/10.1016/j.apcatb.2018.07.029.

References

[1] S.A. Ansari, M.M. Khan, M.O. Ansari, M.H. Cho, Improved electrode performance in microbial fuel cells and the enhanced visible light-induced photoelectrochemical behaviour of PtO x@ M-TiO 2 nanocomposites, Ceram. Int. 41 (2015) 9131–9139.
[2] M. Tahir, C. Cao, N. Mahmood, F.K. Butt, A. Mahmood, F. Idrees, S. Hussain, M. Tanveer, Z. Ali, I. Aslam, Multifunctional g-C3N4 nanofibers: a template-free fabrication and enhanced optical, electrochemical, and photocatalyst properties, ACS Appl. Mater. Interfaces 6 (2013) 1258–1265.
[3] S. Rafqah, A. Aamili, S. Nelieu, L. Kerhoas, J. Einhorn, G. Mailhot, M. Sarakha, Kinetics and mechanism of the degradation of the pesticide metsulfuron methyl induced by excitation of iron (III) aqua complexes in aqueous solutions: steady state and transient absorption spectroscopy studies, Photochem. Photobiol. Sci. 3 (2004) 296–304.
[4] B. AlOtaibi, H. Nguyen, S. Zhao, M. Kibria, S. Fan, Z. Mi, Highly stable photoelectrochemical water splitting and hydrogen generation using a double-band InGaN/GaN core/shell nanowire photoanode, Nano Lett. 13 (2013) 4356–4361.
[5] Y. Wang, X. Li, G. Lu, X. Quan, G. Chen, Highly oriented 1-D ZnO nanorod arrays on zinc foil: direct growth from substrate, optical properties and photocatalytic activities, J. Phys. Chem. C 112 (2008) 7332–7336.
[6] A. Kudo, Y. Miseki, Heterogeneous photocatalyst materials for water splitting, Chem. Soc. Rev. 38 (2009) 253–278.
[7] H. Jun, B. Im, J.Y. Kim, Y.-O. Im, J.-W. Jang, E.S. Kim, J.Y. Kim, H.J. Kang, S.J. Hong, J.S. Lee, Photoelectrochemical water splitting over ordered honeycomb hematite electrodes stabilized by alumina shielding, Energy Environ. Sci. 5 (2012) 6375–6382.
[8] H. Huang, L. Lu, J. Wang, J. Yang, S.-F. Leung, Y. Wang, D. Chen, X. Chen, G. Shen, D. Li, Performance enhancement of thin-film amorphous silicon solar cells with low cost nanodent plasmonic substrates, Energy Environ. Sci. 6 (2013) 2965–2971.
[9] Y.-S. Chen, J.S. Manser, P.V. Kamat, All solution-processed lead halide perovskite-BiVO4 tandem assembly for photolytic solar fuels production, J. Am. Chem. Soc. 137 (2015) 974–981.
[10] S. Thomas, C.-W. Chen, M. Kondiba, C.-Y. Wang, H.-W. Tsai, Z. Wang, Y.-L. Chueh, Recent developments in the synthesis of nanostructured chalcopyrite materials and their applications: a review, RSC Adv. (2016), https://doi.org/10.1039/C6RA05502H.
[11] V. Malik, M. Pokhriyal, S. Uma, Single step hydrothermal synthesis of beyerite, CaBi 2 O 2 (CO 3) 2 for the fabrication of UV-visible light photocatalyst BiOI/CaBi 2 O 2 (CO 3) 2, RSC Adv. 6 (2016) 38252–38262.
[12] G. Liu, P. Niu, L. Yin, H.-M. Cheng, α-Sulfur crystals as a visible-light-active photocatalyst, J. Am. Chem. Soc. 134 (2012) 9070–9073.
[13] W. Li, J. Yue, F. Hua, C. Feng, Y. Bu, Z. Chen, Enhanced visible light photocatalytic property of red phosphorus via surface roughening, Mater. Res. Bull. 70 (2015) 13–19.
[14] G. Liu, P. Niu, H.M. Cheng, Visible-light-active elemental photocatalysts, ChemPhysChem 14 (2013) 885–892.
[15] Z. Hu, L. Yuan, Z. Liu, Z. Shen, J.C. Yu, An elemental phosphorus photocatalyst with a record high hydrogen evolution efficiency, Angew. Chemie (2016), https://doi.org/10.1002/anie.201603331.
[16] H. Dang, X. Dong, Y. Dong, H. Fan, Y. Qiu, Enhancing the photocatalytic H 2 evolution activity of red phosphorous by using noble-metal-free Ni (OH) 2 under photoexcitation up to 700 nm, RSC Adv. 4 (2014) 44823–44826.

[17] Z. Hu, L. Yuan, Z. Liu, Z. Shen, J.C. Yu, An elemental phosphorus photocatalyst with a record high hydrogen evolution efficiency, Angew. Chemie 128 (2016) 9732–9737.
[18] Z. Hu, Z. Shen, C.Y. Jimmy, Phosphorus containing materials for photocatalytic hydrogen evolution, Green Chem. 19 (2017) 588–613.
[19] H.U. Lee, S.C. Lee, J. Won, B.-C. Son, S. Choi, Y. Kim, S.Y. Park, H.-S. Kim, Y.-C. Lee, J. Lee, Stable semiconductor black phosphorus (BP)@ titanium dioxide (TiO2) hybrid photocatalysts, Sci. Rep. 5 (2015).
[20] Y.-P. Yuan, S.-W. Cao, Y.-S. Liao, L.-S. Yin, C. Xue, Red phosphor/gC 3 N 4 heterojunction with enhanced photocatalytic activities for solar fuels production, Appl. Catal., B 140 (2013) 164–168.
[21] N. Comsup, J. Panpranot, P. Praserthdam, The effect of phosphorous precursor on the CO oxidation activity of P-modified TiO 2 supported Ag catalysts, Catal. Commun. 11 (2010) 1238–1243.
[22] X. Wang, K. Maeda, A. Thomas, K. Takanabe, G. Xin, J.M. Carlsson, K. Domen, M. Antonietti, A metal-free polymeric photocatalyst for hydrogen production from water under visible light, Nat. Mater. 8 (2009) 76–80.
[23] X. Wang, K. Maeda, X. Chen, K. Takanabe, K. Domen, Y. Hou, X. Fu, M. Antonietti, Polymer semiconductors for artificial photosynthesis: hydrogen evolution by mesoporous graphitic carbon nitride with visible light, J. Am. Chem. Soc. 131 (2009) 1680–1681.
[24] C. Ye, J.-X. Li, Z.-J. Li, X.-B. Li, X.-B. Fan, L.-P. Zhang, B. Chen, C.-H. Tung, L.-Z. Wu, Enhanced driving force and charge separation efficiency of protonated g-C3N4 for photocatalytic O2 evolution, ACS Catal. 5 (2015) 6973–6979.
[25] K. Zhu, W. Wang, A. Meng, M. Zhao, J. Wang, M. Zhao, D. Zhang, Y. Jia, C. Xu, Z. Li, Mechanically exfoliated gC 3 N 4 thin nanosheets by ball milling as high performance photocatalysts, RSC Adv. 5 (2015) 56239–56243.
[26] S. Yang, Y. Gong, J. Zhang, L. Zhan, L. Ma, Z. Fang, R. Vajtai, X. Wang, P.M. Ajayan, Exfoliated graphitic carbon nitride nanosheets as efficient catalysts for hydrogen evolution under visible light, Adv. Mater. 25 (2013) 2452–2456.
[27] J. Yang, X.W. Xu, Antibacterial activity of TiO2/AgY composite materials, advanced materials research, Trans. Tech. Publ. (2013) 25–28.
[28] T. Muhmood, M.A. Khan, M. Xia, W. Lei, F. Wang, Y. Ouyang, Enhanced photo-electrochemical, photo-degradation and charge separation ability of graphitic carbon nitride (g-C3N4) by self-type metal free heterojunction formation for antibiotic degradation, J. Photochem. Photobiol. A 348 (2017) 118–124.
[29] Y.P. Yuan, S.W. Cao, Y.S. Liao, L.S. Yin, C. Xue, Red phosphor/g-C 3 N 4 heterojunction with enhanced photocatalytic activities for solar fuels production, Appl. Catal. B Environ. 140–141 (2013) 164–168.
[30] X. Wang, K. Maeda, A. Thomas, K. Takanabe, G. Xin, J.M. Carlsson, K. Domen, M. Antonietti, A metal-free polymeric photocatalyst for hydrogen production from water under visible light, Nat. Mater. 8 (2009) 76.
[31] J. Song, Z. Yu, M.L. Gordin, S. Hu, R. Yi, D. Tang, T. Walter, M. Regula, D. Choi, X. Li, Chemically bonded phosphorus/graphene hybrid as a high performance anode for sodium-ion batteries, Nano Lett. 14 (2014) 6329–6335.
[32] L. Jing, R. Zhu, D.L. Phillips, J.C. Yu, Effective prevention of charge trapping in graphitic carbon nitride with nanosized red phosphorus modification for superior photo (electro) catalysis, Adv. Funct. Mater. 27 (2017).
[33] Y.-P. Yuan, S.-W. Cao, Y.-S. Liao, L.-S. Yin, C. Xue, Red phosphor/g-C3N4 heterojunction with enhanced photocatalytic activities for solar fuels production, Appl. Catal. B 140 (2013) 164–168.
[34] T. Muhmood, M. Xia, W. Lei, F. Wang, M.A. Khan, Efficient and stable ZrO2/Fe modified hollow-C3N4 for photodegradation of the herbicide MTSM, RSC Adv. 7 (2017) 3966–3974.
[35] H. Li, L. Zhou, L. Wang, Y. Liu, J. Lei, J. Zhang, Growth of TiO nanocrystals on g-C N for enhanced photocatalytic performance, PCCP 17 (2015) 17406–17412.
[36] S.A. Ansari, M.H. Cho, Highly visible light responsive, narrow band gap TiO2 nanoparticles modified by elemental red phosphorus for photocatalysis and photoelectrochemical applications, Sci. Rep. 6 (2016) 25405.
[37] Y.-P. Zhu, T.-Z. Ren, Z.-Y. Yuan, Mesoporous phosphorus-doped g-C3N4 nanostructured flowers with superior photocatalytic hydrogen evolution performance, ACS Appl. Mater. Interfaces 7 (2015) 16850–16856.
[38] S.A. Ansari, M.M. Khan, M.O. Ansari, M.H. Cho, Gold nanoparticles-sensitized wide and narrow band gap TiO 2 for visible light applications: a comparative study, New J. Chem. 39 (2015) 4708–4715.